

Quantitative phosphoproteomics reveals ectopic ATP synthase on mesenchymal stem cells to promote tumor progression *via* ERK/c-Fos pathway activation

Authors

Yi-Wen Chang, Chia-Chi Wang, Chieh-Fan Yin, Chang-Hsun Wu, Hsuan-Cheng Huang, and Hsueh-Fen Juan

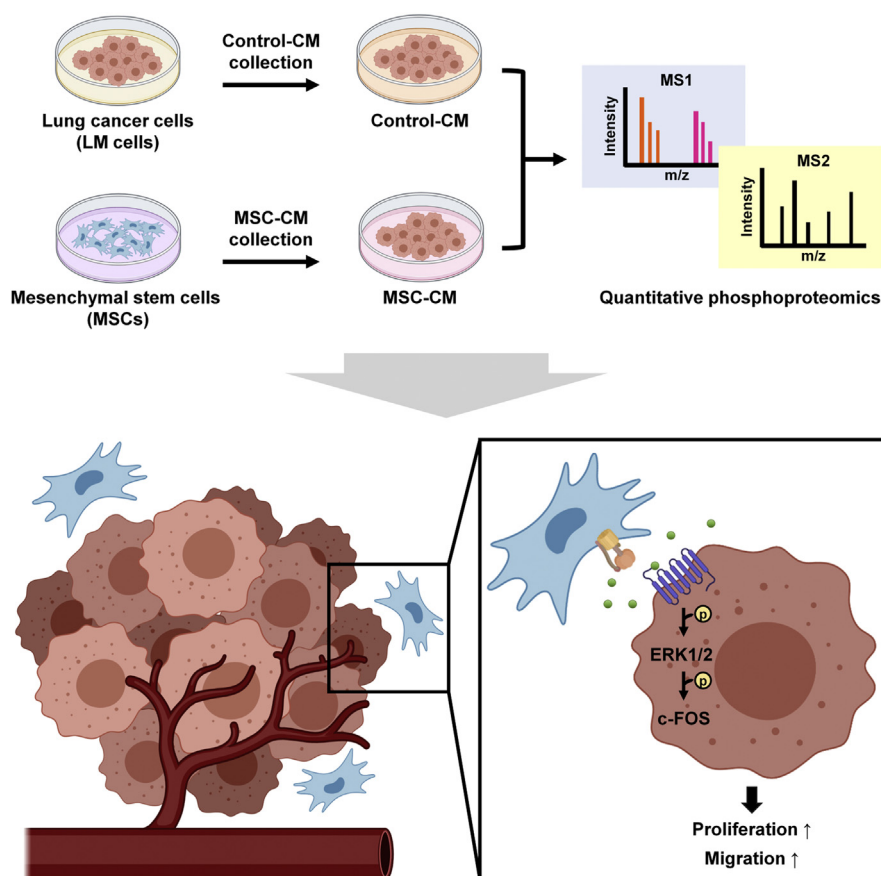
Correspondence

hsuancheng@nycu.edu.tw;
yukijuan@ntu.edu.tw

In Brief

Accumulating studies demonstrate that mesenchymal stem cells (MSCs) within the tumor microenvironment (TME) play crucial roles in cancer development. The intercellular modulating network between MSCs and lung cancer cells is still unclear. Here, quantitative phosphoproteomics is performed to uncover the phosphosignaling pathway regulated by MSC paracrine factors. Our results suggest that ecto-ATP synthase on the cell surface of MSCs generates eATP into the TME. This eATP enhanced proliferation and migration in lung cancer by activating P2X7R/ERK/phospho-c-Fos-S374 pathway.

Graphical Abstract



Highlights

- Mesenchymal stem cells (MSCs) enhance lung cancer development through extracellular factor secretion.
- Phosphoproteomics discover MSCs-regulated phosphosignaling in the lung cancer.
- Ectopic ATP synthase on MSCs surface produces ATP into the tumor microenvironment.
- MSC-secreted extracellular ATP mediates the phosphorylation of the ERK/c-Fos axis.

Quantitative phosphoproteomics reveals ectopic ATP synthase on mesenchymal stem cells to promote tumor progression *via* ERK/c-Fos pathway activation

Yi-Wen Chang¹, Chia-Chi Wang¹, Chieh-Fan Yin¹, Chang-Hsun Wu¹, Hsuan-Cheng Huang^{2,*}, and Hsueh-Fen Juan^{1,3,4,5,*}

The tumor microenvironment (TME), which comprises cellular and noncellular components, is involved in the complex process of cancer development. Emerging evidence suggests that mesenchymal stem cells (MSCs), one of the vital regulators of the TME, foster tumor progression through paracrine secretion. However, the comprehensive phosphosignaling pathways that are mediated by MSC-secreting factors have not yet been fully established. In this study, we attempt to dissect the MSC-triggered mechanism in lung cancer using quantitative phosphoproteomics. A total of 1958 phosphorylation sites are identified in lung cancer cells stimulated with MSC-conditioned medium. Integrative analysis of the identified phosphoproteins and predicted kinases demonstrates that MSC-conditioned medium functionally promotes the proliferation and migration of lung cancer *via* the ERK/phospho-c-Fos-S374 pathway. Recent studies have reported that extracellular ATP accumulates in the TME and stimulates the P2X7R on the cancer cell membrane *via* purinergic signaling. We observe that ectopic ATP synthase is located on the surface of MSCs and excreted extracellular ATP into the lung cancer microenvironment to trigger the ERK/phospho-c-Fos-S374 pathway, which is consistent with these previous findings. Our results suggest that ectopic ATP synthase on the surface of MSCs releases extracellular ATP into the TME, which promotes cancer progression *via* activation of the ERK/phospho-c-Fos-S374 pathway.

The tumor microenvironment (TME), which contributes to tumor formation and progression (1), consists of tumor cells and a variety of tumor-associated stromal cells (2–4). In addition to the cellular components, noncellular components secreted from tumor or stromal cells, such as growth factors, chemokines, cytokines, and extracellular matrix proteins, also

play essential roles in the TME (5, 6). The cross talk between each component in the TME is dynamic, and this is reflected in every phase of cancer pathogenesis (7, 8). Tumor-associated stromal cells, which surround the malignant tumor tissue, include cell types such as stromal fibroblasts, endothelial cells, macrophages, immune cells, and mesenchymal stem cells (MSCs). MSCs are considered multipotent stromal cells that have the potential to differentiate into multiple cell lineages, including osteoblasts, chondrocytes, and adipocytes (9, 10). An increasing number of studies have reported that MSCs could be attracted to the tumor site and cause tumor cells to undergo functional modulation *via* paracrine factors secreted by MSCs or *via* direct interaction with tumor cells (11). For instance, at the primary tumor site, MSCs can enhance tumor invasiveness and metastasis in several cancer types (12–16). Furthermore, at the secondary tumor site, MSCs help metastatic cancer cells to colonize distant organs during the tumor dissemination process (17, 18). Thus, understanding the intercellular communication network between tumor cells and MSCs within the tumor stroma may provide a new avenue for the development of anticancer therapies.

Recent investigations into ectopic adenosine 5'-triphosphate (ATP) synthase (ecto-ATP synthase) highlight the importance of this cell-surface protein in many diseases. Ecto-ATP synthase is an enzyme complex that has been observed on the outer surface of the plasma membrane of various cell types (19, 20). Similar to the structural organization of mitochondrial ATP synthase, ecto-ATP synthase is composed of two major domains, F₁ and F_o (21). The F₁ region consists of three repetitions of subunits α and β and one repetition of subunits γ , δ , and ϵ ($\alpha_3\beta_3\gamma\delta\epsilon$). The F_o region contains subunits a, b, d, F6, oligomycin sensitivity-conferring protein, and a transmembrane c-ring (22). From a functional point of view,

From the ¹Department of Life Science, Institute of Molecular and Cellular Biology, National Taiwan University, Taipei, Taiwan; ²Institute of Biomedical Informatics, National Yang Ming Chiao Tung University, Taipei, Taiwan; ³Graduate Institute of Biomedical Electronics and Bioinformatics, ⁴The Research Center of Developmental Biology and Regenerated Medicine, and ⁵Center for Computational and Systems Biology, National Taiwan University, Taipei, Taiwan

*For correspondence: Hsueh-Fen Juan, yukijuan@ntu.edu.tw; Hsuan-Cheng Huang, hsuancheng@nycu.edu.tw.

ecto-ATP synthase retains the catalytic activity of ATP synthase to phosphorylate ADP and generate extracellular ATP (eATP) (23, 24). Accumulating evidence seems to suggest that the concentration of eATP in tumor tissue is vital for the determination of cell growth, invasion, and even chemoresistance (25, 26). Moreover, our previous data have shown that ecto-ATP synthase blockade consequently inhibits the proliferation of various tumor cells (27–29). Therefore, clarification of the role of ecto-ATP synthase in the TME may give new insight into the development of therapeutic strategies for cancer.

Recent cancer research suggests that P2X purinergic receptors (P2XRs) act as the specific plasma membrane receptors for eATP (30, 31). In response to stimulation with eATP, P2XRs trigger intracellular signal transduction cascades to control multiple physiological and pathophysiological processes (32). Among the P2XR family, the P2X purinergic receptor 7 (P2X7R) subtype is commonly overexpressed in most malignant tumor cells, including those of primary breast cancers, prostate cancers, melanoma, colon cancers, neuroblastoma, and non-small cell lung carcinoma (33, 34). The stimulation of P2X7Rs, located on the cell surfaces of cancer cells, by eATP in the TME activates either the PI3K-AKT pathway or the ERK1/2-MAPK pathway, both of which are involved in the regulation of tumor growth (35–39). In addition to mediating the P2X7R-dependent signaling pathway, the stimulation of P2X7R also enhances the release of cytokines and matrix metalloproteinases to promote tumor cell motility, migration, and invasion (40–42). Several pre-clinical studies suggest that the targeting of P2X7Rs may serve as a potent option for cancer therapy (43, 44). In this study, MSC-culture medium was collected and used to treat lung cancer cells in order to analyze the tumor functions that are regulated by the paracrine factors secreted by MSCs. A time-series phosphoproteomic analysis was performed to further improve our understanding of the molecular mechanisms triggered by MSCs in cancer. These results may provide new insights into the TME and thus be useful for improving cancer therapy.

EXPERIMENTAL PROCEDURES

Cell Culture

MSCs expressing red fluorescent protein (hTERT/RFP-cbMSCs, abbreviated as MSCs hereafter) (45) and A549 lung cancer cells were purchased from the Bioresource Collection and Research Center (Food Industry Research and Development Institute, Hsinchu, Taiwan). Low-motility cells (LM cells) were selected via a Transwell migration assay from the A549 cell line, as per the methods outlined in a previous study (46). MSCs were cultured in minimum essential medium (MEM, Gibco Laboratories) supplemented with 20% fetal bovine serum (FBS; Gibco Laboratories), 4 ng/ml human fibroblast growth factor-basic, 1 mM sodium pyruvate (Thermo Fisher Scientific), 30 µg/ml hygromycin (Millipore), and 200 µg/ml geneticin (Millipore). A549, CL1-0, and LM cells were grown in Dulbecco's modified Eagle's medium (DMEM; Gibco Laboratories) supplemented with 10% FBS. All cell lines were cultured in an incubator at 37 °C and with 5% CO₂.

Cell lines used in this study were authenticated by short tandem repeat profiling and tested for *Mycoplasma* contamination.

Conditioned Medium Collection

MSCs (1×10^6) were plated in 10-cm culture dishes in MEM containing 20% FBS. After culturing for 72 h, the culture medium from the MSCs (MSC-CM) was collected and then centrifuged for 10 min at 2000g to remove cell debris. The supernatant was stored at –80 °C. The culture medium from the same number of A549 or LM cells was collected as Control-CM. The culture medium from MSCs or lung cancer cells treated with ecto-ATPi, citreoviridin, for 72 h was collected as ecto-ATPi-Control-CM or ecto-ATPi-MS-CM.

Antibodies and Reagents

The antibodies used in this study were as follows: anti-phospho-c-Fos (pSer374) (Santa Cruz Biotechnology), anti-c-Fos (Cell Signaling Technology), anti-phospho-ERK1/2 (pThr202/pTyr204; Cell Signaling Technology), anti-ERK1/2 (Cell Signaling Technology), anti-HA (Biolegend), anti-GAPDH (Millipore), anti-β-actin (Millipore), horseradish peroxidase-conjugated anti-rabbit IgG H&L (Abcam), and horseradish peroxidase-conjugated anti-mouse IgG H&L (Abcam). ERK1/2 inhibitor (SCH772984; TargetMol) and competitive P2X7R antagonist (A 438079; Abcam) were dissolved in DMSO (Sigma-Aldrich) and stored at –20 °C.

Cell Proliferation Analysis

Cells were seeded onto six-well plates at 4×10^4 cells per well. After attachment for 24 h, the culture medium was replaced with serum-free DMEM for 24 h. The cells were then incubated with MSC-CM for the indicated time points. Cell viabilities were identified through 0.4% trypan blue solution (VWR), and the total number of viable cells for each well was measured using a hemocytometer. Cells incubated with Control-CM served as control groups.

MTS Assay

Cells were seeded onto 96-well plates at 1×10^3 cells per well. At the indicated time points, cell viability was detected in the MSC-CM and Control-CM groups using CellTiter 96 Aqueous MTS Reagent (Promega Corporation) according to the manufacturer's protocol. The relative cell viability and raw absorbance values are presented as histograms.

Migration Assay

Cell migration was assessed using a Boyden chamber assay involving an 8-µm pore polycarbonate membrane (Corning Incorporated). Cells (3.5×10^4) were seeded onto six-well plates and stimulated with MSC-CM for 72 h, as per the aforementioned procedure. The pretreated cells were then trypsinized and placed in the plate well inserts at a density of 5×10^4 cells per chamber, and conditioned medium was added into the lower Transwell chambers. After incubation for 10 h, the insert membranes were fixed with 3.7% paraformaldehyde at room temperature for 5 min, followed by 100% MeOH overnight. The cells on the top surface of the inserts were wiped off with cotton swabs, and the migrating cells on the other side of the inserts were stained with 10% Giemsa stain (Sigma-Aldrich) for 1 h. After washing with PBS, the stained migrating cells were observed and counted under a microscope. Five fields were randomly selected for each insert membrane, and the average number of migrating cells in each Transwell chamber was represented in bar charts.

Colony Forming Assay

Cells were seeded onto six-well plates at 1×10^3 cells per well and adhered for 24 h. Cells were then incubated with serum-free DMEM for

24 h before being treated with MSC-CM for 14 days for colony formation (fresh MSC-CM was exchanged every 3 days). Colonies were fixed with 100% methanol and stained with 10% Giemsa stain. The colony numbers were quantified using ImageJ (National Institutes of Health).

Experimental Design and Statistical Rationale

LM cells were treated with MSC-CM or with Control-CM for 5 min, 10 min, 30 min, and 60 min. The Control-CM-treated cells served as controls. Two biological replicates of the Control-CM-treated and the MSC-CM-treated LM cells for each time point were obtained, and each biological sample underwent duplicate nanoLC-MS/MS analyses. Phosphosites with differential phosphorylation levels were assessed using ANOVA analysis.

Protein Extraction

The Control-CM-treated cells and the MSC-CM-treated cells were lysed by using PTS lysis buffer composed of 12 mM sodium deoxycholate (Sigma-Aldrich), 12 mM sodium lauroyl sarcosinate (MP Bio-medicals), and 50 mM triethylammonium bicarbonate (TEAB; Sigma-Aldrich) (47). Protease inhibitor cocktail (BioShop), phosphatase inhibitor cocktail I (tyrosine phosphatase inhibitors; BioShop), and phosphatase inhibitor cocktail II (serine/threonine phosphatase inhibitors; BioShop) were added into the PTS lysis buffer for the protection of proteins and phosphoproteins. Proteins were extracted using an ultrasonic homogenizer (LABSONIC M ultrasonic homogenizer, Sartorius AG) operating at 60% amplitude and 0.6 cycle duration for 2 min. After centrifugation at 16,000g for 20 min, the supernatants were transferred into new Eppendorf tubes. The concentrations of the proteins of interest were detected using a Pierce BCA Protein Assay Kit (Thermo Fisher Scientific) according to the manufacturer's instructions.

Sample Preparation for Quantitative Phosphoproteomics

Five hundred micrograms of each protein sample was reduced with 10 mM dithiothreitol (DTT; BioShop) at room temperature for 30 min, and cysteines were carbamidomethylated with 55 mM iodoacetamide (Sigma-Aldrich) in the dark at room temperature for 30 min. Proteins were digested with Lys-C (1:100 w/w; WAKO) for 2 h, followed by digestion with MS-grade trypsin (1:100 w/w; Thermo Fisher Scientific) for 16 h at 37 °C. An immiscible organic solvent, ethyl acetate (Sigma-Aldrich), was mixed into the digested peptide samples for the purposes of detergent removal (48). After centrifuging at 15,700g for 2 min, the aqueous samples (with the detergent removed) were desalted by using homemade SDB-XC StageTips (3M) (49). One hundred micrograms of peptide was dried under vacuum and then dissolved in 100 µl of 100 mM TEAB solution and labeled. The peptides obtained from both the Control-CM-treated group and the MSC-CM-treated group for each time point were labeled with 4% formaldehyde-H₂ (Sigma-Aldrich) and 4% formaldehyde-D₂ (Sigma-Aldrich), respectively. Freshly prepared 0.6 M sodium cyanoborohydride (Sigma-Aldrich) was added as a catalyst. Cold 1% (v/v) ammonium hydroxide (WAKO) was added to stop the dimethyl labeling reaction, and 10% (v/v) trifluoroacetic acid (TFA; Sigma-Aldrich) was used to acidify the isotope-labeled peptides to pH < 3 (50). Finally, an equal volume of H₂-labeled peptides (Control-CM group) and D₂-labeled peptides (MSC-CM group) were combined and then desalted with homemade SDB-XC StageTips. The phosphopeptides were enriched by hydroxy acid-modified metal oxide chromatography (MOC) using homemade MOC tips that were prepared by packing 1 mg of TiO₂ beads (GL Sciences) into 10-µl C8 StageTips (49, 51, 52). The isotope-labeled peptide mixture was combined with an equal volume of solution A (0.1% TFA, 80% acetonitrile [Thermo Fisher Scientific] and

300 mg/ml lactic acid [WAKO]) and then loaded onto MOC tips (100 µg peptide/tip) that were equilibrated with solution A after being pre-conditioned with solution B (0.1% TFA and 80% acetonitrile). After washing with solution A and solution B, the phosphopeptides were eluted with 0.5% and 5% piperidine (Sigma-Aldrich), acidified, and desalted. Each sample was dried with a centrifugal evaporator before being analyzed by nanoLC-MS/MS.

NanoLC-MS/MS Analysis

LTQ-Orbitrap XL (Thermo Fisher Scientific) coupled with a nano-AQUITY UPLC system (Waters) was used to perform the NanoLC-MS/MS analysis. In brief, samples were loaded into a 2-cm × 180-µm capillary trap column and then separated in a C18 BEH nano-AQUITY column with an internal diameter (I.D.) of 75 µm and a length of 25 cm, at a flow rate of 300 nl/min, where mobile phases were the mixture of buffer A (0.1% formic acid [WAKO]) and buffer B (0.1% formic acid and 80% acetonitrile). Buffer A linear gradient of 10 to 40% buffer B in 90 min and later 40 to 85% buffer B in 10 min was applied throughout this study. Mass spectra from a full survey scan were acquired using the Orbitrap (*m/z* 300–1500). The resolution of the instrument was set to 60,000 at *m/z* 400 with an automated gain control value of 10⁶. The top 10 most intense precursor ions were selected from the MS scan for subsequent collision-induced dissociation MS/MS scanning by ion trap (with an automated gain control target of 7000).

Identification, Quantification, and Analysis of Mass Spectrometric Data

Raw MS/MS spectrums were analyzed using MaxQuant software version 1.5.2.8 (<http://maxquant.org/>) following parameters used in previous studies (53): trypsin specificity allowing for up to two missed cleavage sites; carbamidomethylation on cysteine (C) was set as fixed modification; oxidation on methionine (M) and phosphorylation on serine, threonine, or tyrosine residues (STY) were selected as variable modifications. The minimal peptide length was set at seven amino acids. The first search peptide tolerance was 20 ppm, whereas the main search peptide tolerance was 4.5 ppm. Fourier transform-based mass spectrometry MS/MS match tolerance was set as 20 ppm. Peptide identification was performed using the Andromeda search engine against the 20,386 UniProtKB/SwissProt human protein entries published on Jun, 02, 2021 (54). A false discovery rate of 1%, searching against a randomized target-decoy database created by MaxQuant, was applied for peptide, protein, and site identifications. The intensity value of dimethyl-labeled phosphopeptides was obtained by summing up the eXtracted Ion Current (XIC) in two technical replicates. The normalized ratios of the heavy-light dimethyl-labeled partners (MSC-CM treatment *versus* Control-CM treatment) were reported by MaxQuant using the robust linear regression of the 2D centroid intensities of isotope pairs and adjusting the median of logarithmized ratios to 0 (55). The normalized ratios were estimated in two biological replicates. A site localization probability of 0.75 was set as the threshold for localization of phosphorylation sites. The significantly regulated phosphosites between the MSC-CM and the Control-CM groups were determined by ANOVA with a *p*-value cutoff 0.05 in the Perseus environment using default parameters (version 1.6.1.3) (56). To discover the kinase activities in response to MSC-CM treatment, a literature-based kinase-substrate library, Kinase Enrichment Analysis (KEA2), was applied with the default setting (57). Benjamini-Hochberg false discovery rate was used to adjust the *p*-values for multiple test correction. The predicted kinases and their substrates (only MSC-CM-regulated phosphosites were shown) were employed to construct the kinase-substrate network, which was visualized in Cytoscape (version 3.7.1). All edges represent the known kinase-substrate interactions in the literature.

Plasmid Construction and Transfection

The open reading frame (ORF) region of the human *FOS* gene (NM_005252.4) was amplified by PCR using Phusion High-Fidelity DNA Polymerase (Thermo Fisher Scientific). Primers for amplifying wildtype c-Fos and mutant c-Fos (c-Fos-S374A) sequences were as follows: forward, 5'-ATGGAGGCCCGAATCCCACCATGATGTTCTCGGGCTTC; reverse, 5'-CTGGATCCCCGCGGCCGCTCACAGGGCCAGCAGCGTGGTGAGCTGAGCG (wildtype c-Fos); forward, 5'-ATGGAGGCCCGAATCCCACCATGATGTTCTCGGGCTTC; reverse, 5'-CTGGATCCCCGCGGCCGCTCACAGGGCCAGCAGCGTGGTGAGCTGAGCG (mutant c-Fos). PCR products were purified with Zymoclean Gel DNA Recovery Kit (Zymo Research), cloned into a linear pCMV-HA-N vector (Takara Bio), and digested by EcoRI and NotI (FastDigest; Thermo Fisher Scientific). The mutant c-Fos (c-Fos-S374A) was generated through site-directed mutagenesis using wildtype c-Fos. Constructions were transfected into cells with jetPRIME *in vitro* DNA and siRNA transfection reagent (Polyplus-transfection SA) according to the manufacturer's instructions. After incubation for 24 h, the transfected cells were subjected to further experimentation.

Fluorescent Immunocytochemistry

MSCs were seeded at a density of 2.5×10^4 cells per well onto coverslips placed in 12-well culture dishes. MitoTracker (200 nM, Thermo Fisher Scientific) was used for labeling mitochondria in both the permeabilized and nonpermeabilized groups. After fixation with 3.7% paraformaldehyde (Sigma-Aldrich), cells on the coverslips were blocked in 5% bovine serum albumin (BioShop) in Tris-buffered saline (TBS; 50 mM Tris, 150 mM NaCl, pH 7.2–7.4) with or without 0.1% Triton X-100 (Sigma-Aldrich). Cells were then hybridized with antibodies against ATP synthase complex (Abcam) or IgG (Abcam) overnight at 4 °C. IgG antibody was used for excluding the nonspecific signals. After washing with TBS to eliminate nonspecific binding, the coverslips were incubated with Alexa Fluor 488-conjugated goat anti-mouse IgG secondary antibody (Abcam) and mounted onto the glass slides with the blue DNA stain DAPI (Thermo Fisher Scientific). Images were taken using a Zeiss LSM 780 laser scanning confocal microscope and adjusted with Zen 2.6 software (blue edition).

Flow Cytometry

MSCs (1×10^6) were seeded onto 10-cm culture dishes and incubated for 72 h. Cells were detached with 1 mM EDTA (J.T. Baker) and resuspended with MEM containing 20% FBS. After fixation, 1×10^6 MSCs were incubated with anti-ATP synthase complex immunocapture antibody [12F4AD8AF8] (ab109867, Abcam) (58), which is able to detect the native folded whole enzyme, or mouse anti-IgG antibody (ab18457, Abcam) overnight. The cells were then hybridized with Alexa Fluor 488-conjugated goat anti-mouse IgG secondary antibody (Abcam) by rotation for 2 h at room temperature. Triton X-100 (0.1%) in PBS was used for permeabilization. The fluorescence signal was detected using a BD FACSCanto II (BD Biosciences).

ATP Bioluminescence Assay

MSCs were seeded at a density of 2.5×10^4 cells per well in 12-well plates and cultured for 72 h. Cells were pretreated with or without citreoviridin (2 μ M), oligomycin (5 μ g/ml), carbonyl cyanide 3-chlorophenylhydrazone (1 μ M), or P^iP^5 -Di(adenosine-5') pentaphosphate pentasodium salt (A_p^5A) (300 μ M) at 37 °C for 5 min. ATP production was started by adding 100 μ M ADP alone or 100 μ M ADP and 5 mM Pi. After 3 min incubation, the supernatants were collected and centrifuged at 300g for 15 s to stop the reaction. The cell debris was removed by further centrifugation at 2000g for 10 min. An ATP Bioluminescent Assay Kit (Sigma-Aldrich) was used to quantify eATP concentrations, as per the manufacturer's instructions. In brief, 100 μ l

of ATP Assay Mix solution, dissolved in sterile water and adjusted to pH 7.8, was added into each well of the 96-well opaque plate and incubated at room temperature for 3 min to hydrolyze endogenous ATP. The same volume of ATP standards or samples was then added into the wells. After gently swirling, the light was immediately measured by FlexStation three microplate readers (Molecular Devices). A standard curve was prepared by ATP in the range of 8×10^{-8} to 2×10^{-4} M to determine the conditional medium's ATP concentration. The concentration of eATP in the conditioned medium was normalized according to the cell number.

Statistical Analysis

Data are displayed as means \pm SD ($n = 3$). The statistical significance of effects was analyzed using Student's unpaired two-tailed *t* test for two-group comparisons. A *p*-value < 0.05 was considered statistically significant.

RESULTS

MSCs Accelerate Lung Cancer Progression

An increasing number of studies have demonstrated that MSCs possess either protumorigenic or antitumorigenic effects in different types of cancers (59, 60). Therefore, we first investigated the role of MSCs in non-small cell lung cancers. Conditioned medium from MSCs (MSC-CM) was collected and used to treat A549 and LM lung cancer cell lines. The results showed that MSC-CM increased the proliferation rate of lung cancer cells (Fig. 1, A and B). An MTS assay showed that cell viability was consistently higher in lung cancer cells treated with MSC-CM (Fig. 1, C and D). The colony-forming ability of the cells was also enhanced in response to MSC-CM treatment (Fig. 1, E and F). In addition, we investigated whether MSC-CM affected the motility of the cells. In both A549 and LM cells, MSC-CM promoted their Transwell migration ability relative to the Control-CM treatment (Fig. 1, G and H). Here, our results suggest that MSCs enhance proliferation and migration in lung cancer cells through paracrine factors.

Quantitative Phosphoproteomic Profiling Reveals the Temporal Dynamics Behind MSC-Regulated Phosphorylation

After verifying the functional effects of MSC-CM in lung cancer cells, we were curious about the molecular mechanisms induced by MSCs. Hence, we performed quantitative phosphoproteomic profiling, which provides a more holistic insight into protein phosphorylation modification, to explore the signaling pathways triggered by MSC-CM. The proteins of LM cells treated with MSC-CM or Control-CM for 5, 10, 30, or 60 min were extracted and digested. Peptides from the control and treatment groups were labeled with formaldehyde- H_2 or formaldehyde- D_2 , respectively. The phosphopeptides were further enriched with TiO_2 , identified and quantified via nano-scale liquid chromatography-tandem mass spectrometry (nanoLC-MS/MS) and analyzed using a bioinformatics approach (Fig. 2A). We identified a total of 1321 peptides that

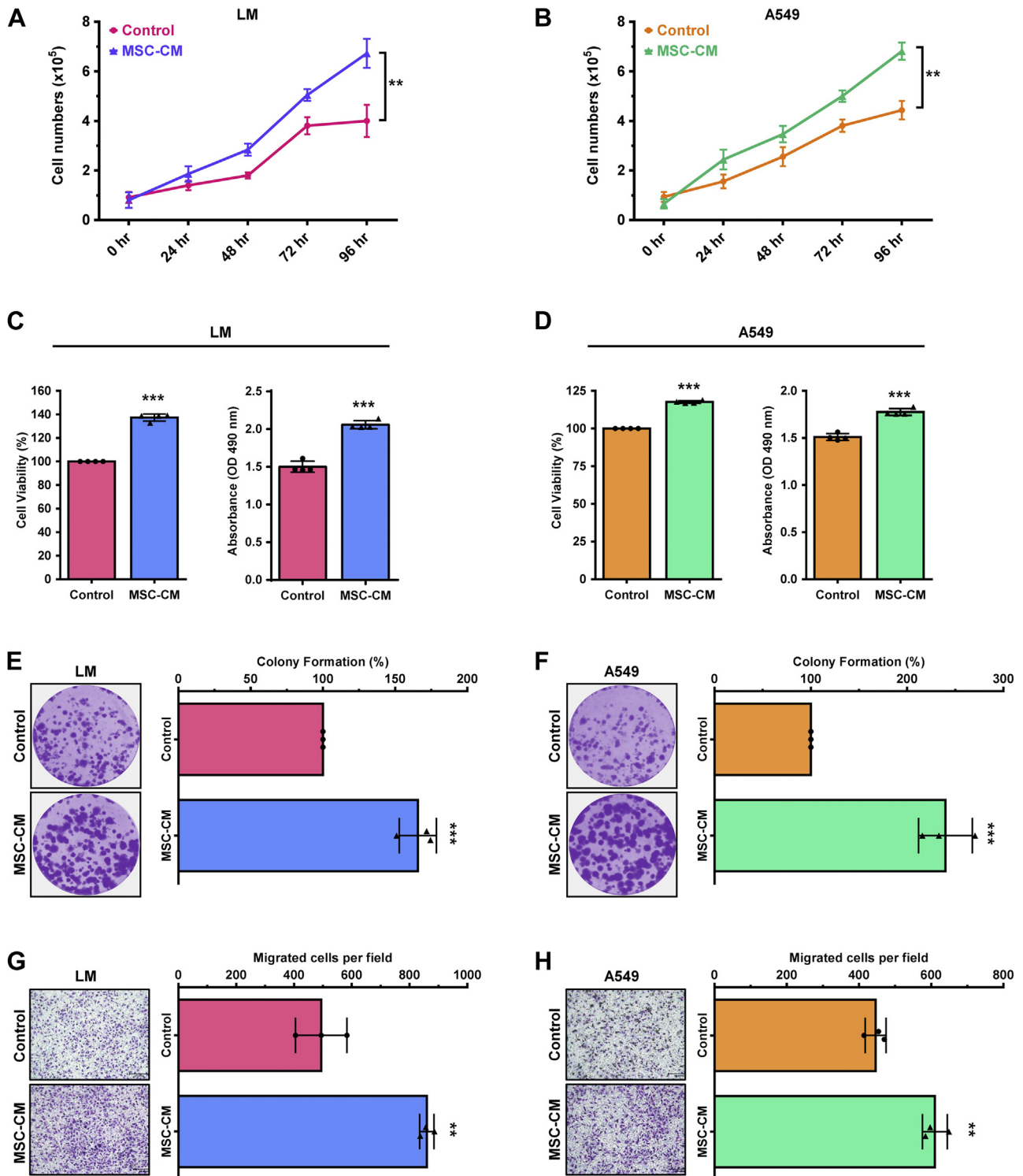


FIG. 1. MSC-CM promotes cell proliferation and migration in lung cancer cells. *A* and *B*, numbers of lung cancer cells treated with Control-CM or MSC-CM at the indicated time points were counted using a hemocytometer. *C* and *D*, cell viability in Control-CM–treated and MSC-CM–treated groups was detected using an MTS assay. The raw 490 nm absorbance values and the relative cell viability percentages are expressed as bar graphs. *E* and *F*, the colony-forming ability of LM and A549 cells treated with or without MSC-CM for 14 days was assessed and is expressed as a percentage relative to the control group. *G* and *H*, a Transwell assay was performed to determine the effect of MSC-CM on tumor cell migration. The average number of migrating cells in each Transwell insert was calculated from five randomly selected fields. Representative images from three independent biological replicates are shown in *E*–*H*, and the quantitative results are displayed as mean ± standard deviation. **p* < 0.05, ***p* < 0.01, ****p* < 0.001, two-tailed *t* test. CM, conditioned medium; LM, low-motility; MSC, mesenchymal stem cell.

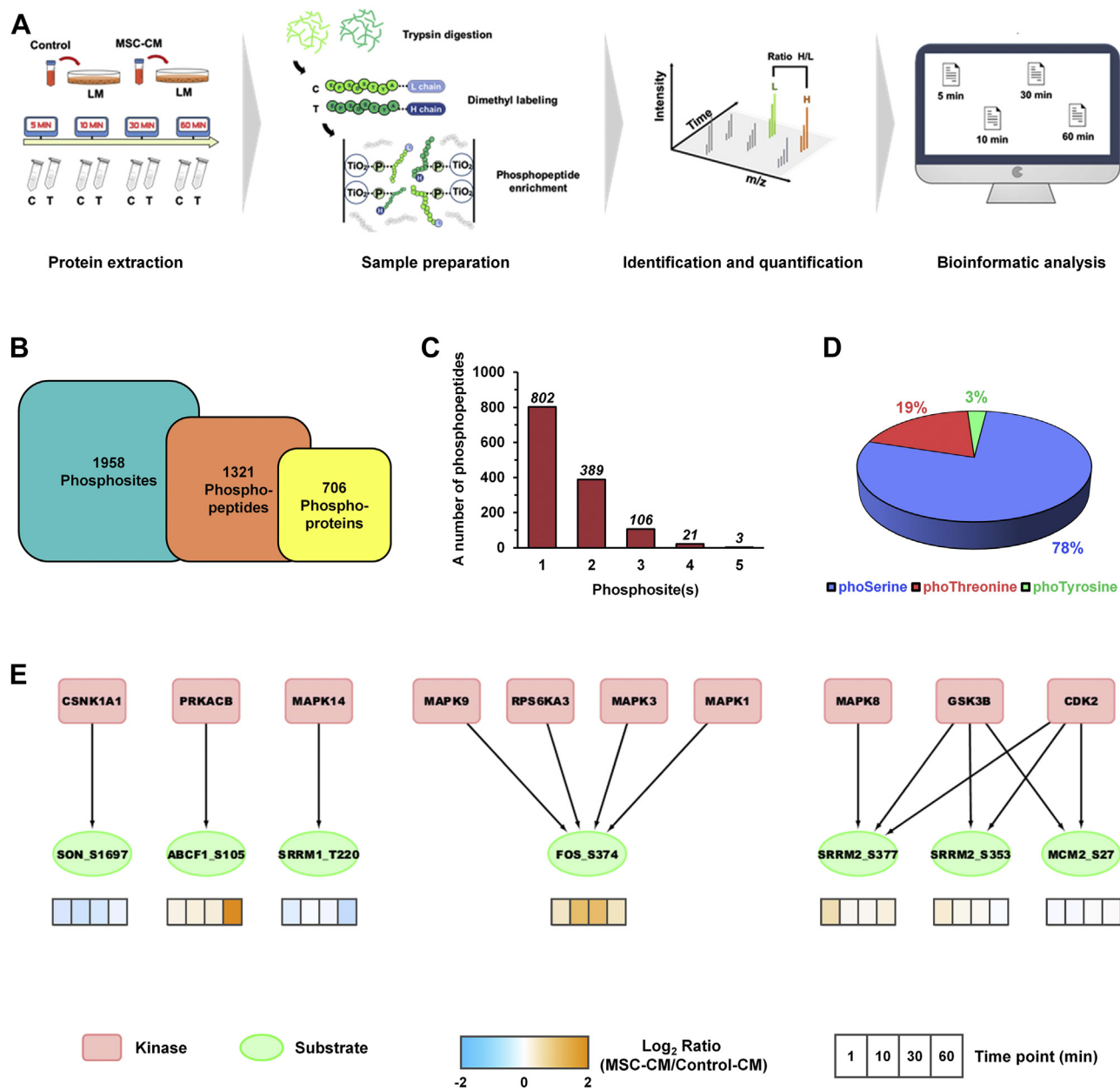


FIG. 2. Identification of phosphorylated proteins in lung cancer cells in response to MSC-CM via quantitative phosphoproteomic analysis. A, the overall workflow for establishing the phosphoproteomic profile of LM cells in response to short-term MSC-CM treatment. T represents the MSC-CM-treated group, and C represents the Control-CM-treated group. B, the total number of identified phosphosites, phosphopeptides, and phosphoproteins across all time points. C, the number of phosphopeptides with singly, doubly, triply, quadruply, and quintuply phosphorylated residues. D, the percentages of phosphorylated serine (phoSerine), threonine (phoThreonine), and tyrosine (phoTyrosine) in all identified phosphosites. E, the kinases associated with the phosphorylated sites that were significantly upregulated after being treated with MSC-CM were predicted and are presented as a kinase-substrate network. The color of squares indicates the relative levels of phosphoproteins (MSC-CM treatment/Control-CM treatment). CM, conditioned medium; LM, low-motility; MSC, mesenchymal stem cell.

contained 1958 phosphorylation sites located on 706 proteins, with 97% phosphopeptide enrichment efficiency (Fig. 2B and supplemental Table S1). Most of the identified phosphopeptides were singly or doubly phosphorylated (Fig. 2C). Among all of the identified phosphosites, 78% were

distributed on serine (pSer), 19% on threonine (pThr), and 3% on tyrosine (pTyr) (Fig. 2D). ANOVA was then used to identify the significantly regulated phosphosites in response to MSC-CM treatment (supplemental Table S2). We then became curious about the kinases that were responsible for these

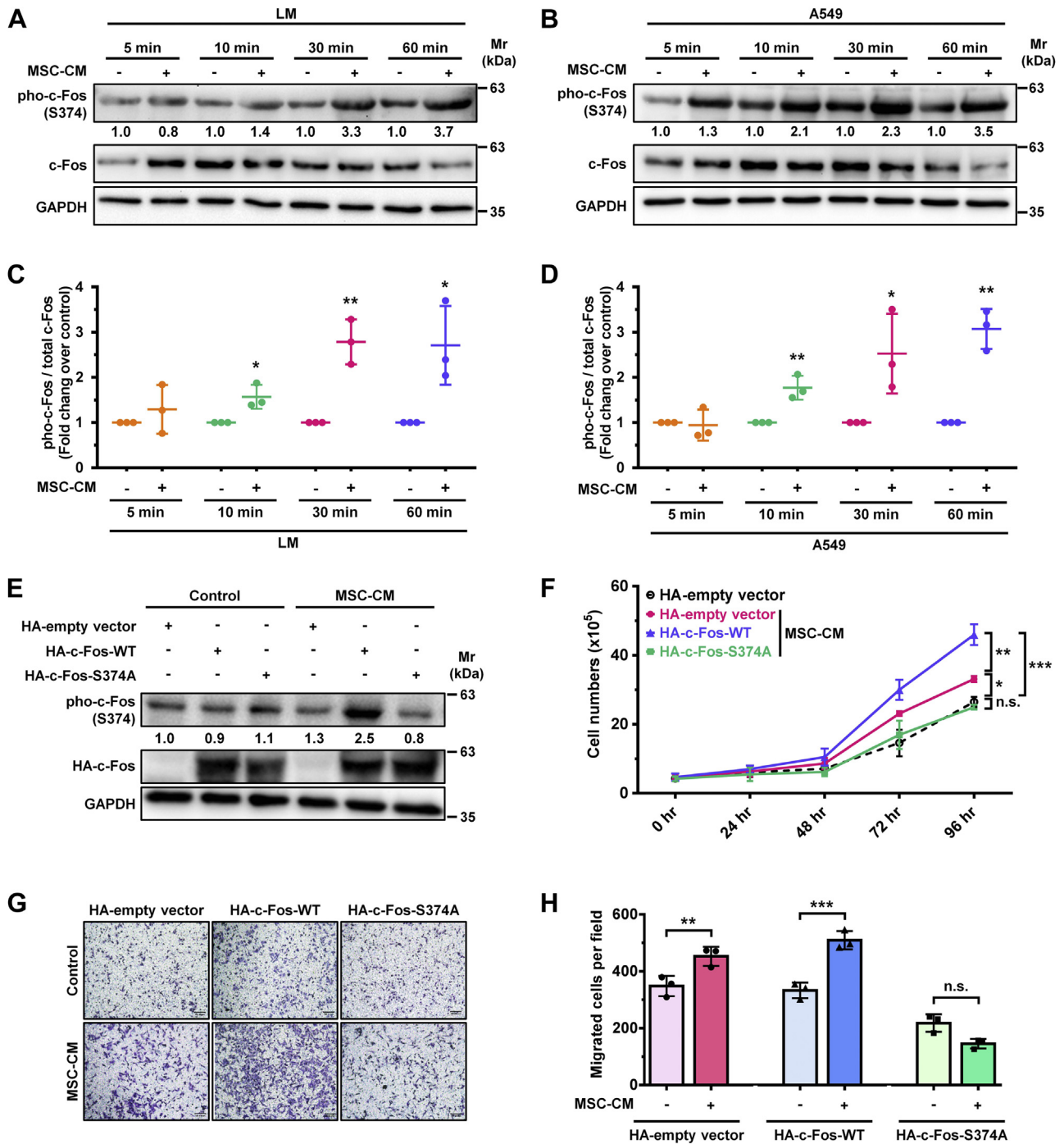


FIG. 3. MSC-CM enhances tumor proliferation and metastasis by increasing phosphorylation of c-Fos at serine 374. A–D, LM cells (A) and A549 cells (B) were treated with Control-CM or MSC-CM at the indicated time points. The total expression levels of c-Fos and phospho-c-Fos-S374 were detected with Western blotting. GAPDH expression levels served as the loading control. The fold changes in phospho-c-Fos-S374 expression between Control-CM-treated and MSC-CM-treated groups were quantified using ImageJ and normalized according to the expression levels of total c-Fos. The quantified results from three biological replicates are displayed as dot plots (C and D). E, cells were transfected with HA-c-Fos-wildtype plasmid or HA-c-Fos-S374A mutation plasmid for 24 h before being treated with MSC-CM. The levels of c-Fos and phospho-c-Fos-S374 were verified using Western blotting and quantified using ImageJ. F, the number of HA-c-Fos-WT and HA-c-Fos-S374A-transfected cells stimulated with or without MSC-CM for 24, 48, 72, or 96 h was counted using a hemocytometer. G and H, HA-c-Fos-WT and HA-c-Fos-S374A-overexpressing cells were treated with Control-CM and MSC-CM, respectively. Their migrating ability was assessed using a Transwell assay. Representative images from three independent biological replicates are shown (G), and the quantitative results are displayed as a histogram (H). **p* < 0.05, ***p* < 0.01, ****p* < 0.001, two-tailed *t* test. CM, conditioned medium; LM, low-motility; MSC, mesenchymal stem cell.

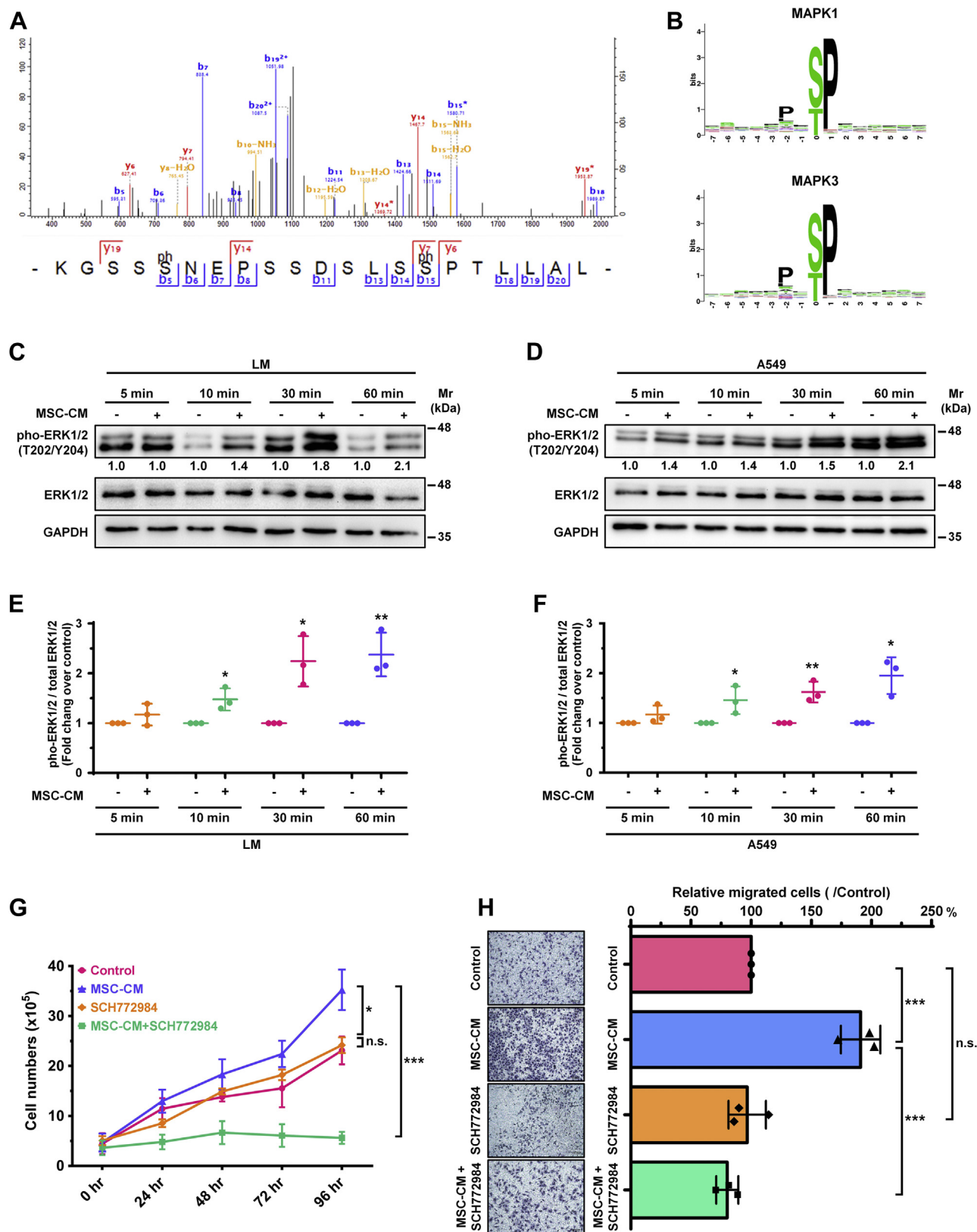


FIG. 4. MSC-CM enhances tumor progression via the activation of the ERK/c-Fos signaling axis. A, the MS/MS spectrum of the phosphopeptide from c-Fos. The fragment ions in the MS² spectrum localized at the phosphorylation site to serine 374. B, the consensus motifs

differential phosphosites. Ten predicted kinases (red rectangles) were enriched and used to construct a kinase–substrate network (Fig. 2E and supplemental Table S3). Among the MSC-mediated phosphosites, the phosphorylation of the proto-oncogene, c-Fos, at serine 374 was approximately doubled in MSC-CM-treated cells at all four time points. Our results imply that the phosphorylation of c-Fos at Ser374 may play a critical role in MSC-triggered tumor progression.

Phosphorylation of c-fos at Serine 374 Plays a Critical Role in MSC-Induced Tumor Progression

Western blotting further verified that the phosphorylation levels at Ser374 in c-Fos were indeed upregulated in MSC-CM-treated cells compared with the control group (Fig. 3, A–D). To determine whether phosphorylation of Ser374 in c-Fos was involved in functions regulated via MSC-CM, a non-phosphorylatable mutation of c-Fos was generated by site-directed mutagenesis of Ser374 to Ala374 in c-Fos. Lung cancer cells were then transfected with either HA-tagged wildtype c-Fos (HA-c-Fos-WT) or a nonphosphorylatable mutation on Ser374 of c-Fos (HA-c-Fos-S374A). Upon treatment of the cells with MSC-CM, the phosphorylation levels of c-Fos at Ser374 were diminished in HA-c-Fos-S374A-transfected cells relative to HA-c-Fos-WT-transfected cells (Fig. 3E). We further assessed the relevance of phosphorylated c-Fos in MSC-CM-triggered functions. In the presence of MSC-CM, both proliferation rate (Fig. 3F) and migration (Fig. 3, G and H) were enhanced in HA-c-Fos-WT-expressing cells, while this was not the case for HA-c-Fos-S374A-expressing cells. These results indicate that both MSC-mediated tumor cell proliferation and cell migration require the phosphorylation of c-Fos at Ser374.

Factors Secreted by MSCs Trigger the Phosphorylation of ERK1/2 to Promote Tumor Progression

As shown in the kinase–substrate network (Fig. 2E), MAPK1, MAPK3, MAPK9, and RPS6KA3 were responsible for the phosphorylation of c-Fos at Ser374. Of these, the consensus phosphorylation motifs of MAPK3 and MAPK1, also known as extracellular signal-regulated protein kinases 1 and 2 (ERK1/2), matched the sequence pattern of c-Fos near Ser374, as identified via mass spectrometry (Fig. 4, A and B). This evidence suggests that ERK1/2 act as the serine/threonine kinases that phosphorylate c-Fos at Ser374. ERK1/2 play an important role in the mitogen-activated protein kinase (MAPK) signal transduction cascade, which is responsible for many

biological functions (61). ERK1/2 are activated by various extracellular stimuli and are subsequently involved in cell proliferation, motility, and survival of cancer cells through the phosphorylation of their downstream transcriptional factors, including c-Fos (62). Therefore, we hypothesized that MSCs activate the ERK1/2–c-Fos signaling axis via the secretion of paracrine factors. The kinase activities of ERK1/2 depend on the phosphorylation status of the threonine 202 and tyrosine 204 residues (63). Therefore, we first validated whether MSC-CM could induce the phosphorylation of ERK1/2 at Thr202 and Tyr204. Western blotting showed that the phosphorylation levels of ERK1/2 at Thr202 and Tyr204 were upregulated in both LM cells (Fig. 4C) and A549 cells (Fig. 4D) after MSC-CM stimulation. These high phosphorylation ratios were normalized by the addition of glyceraldehyde 3-phosphate dehydrogenase (GAPDH), relative to the control group (Fig. 4, E and F). Combining these findings with our results described earlier, we speculated that ERK1/2 might play crucial roles in MSC-CM-mediated tumor progression by elevating the phosphorylation of c-Fos. Hence, SCH772984, as a specific ERK1/2 inhibitor, was applied with MSC-CM to lung cancer cells to suppress the kinase activities of ERK1/2 (64). As expected, SCH772984 cotreatment abrogated MSC-CM-induced cell proliferation (Fig. 4G) and cell migration (Fig. 4H) in the cells. Combining these results, we have illustrated that MSCs promote cell proliferation and motility in lung cancer through phosphorylation of the ERK1/2–c-Fos axis.

ecto-ATP Synthase on the Cell Surface of MSCs Produces eATP in the TME to Induce the ERK/c-Fos Pathway

An increasing number of studies have demonstrated that eATP is released in the TME and enhances tumorigenesis (65, 66). We were curious about whether MSC-CM contains abundant eATP, which would regulate cancer development. We first attempted to elucidate whether ATP stimulation could lead to similar changes in the phosphorylation of the ERK1/2–c-Fos axis as were caused by MSC-CM. Western blotting indicated that the levels of phosphorylation of ERK1/2 at Thr202 and Tyr 204 and in c-Fos at Ser 374 were both increased after ATP stimulation (supplemental Fig. S1, A and B). The relative phosphorylated levels of phospho-ERK1/2-T202/Y204 and phospho-c-Fos-S374 in ATP-treated cells compared to the control group in each time point was normalized according to the level of total ERK1/2 or c-Fos and the loading control (GAPDH) (supplemental Fig. S1, C–F). Emerging evidence has proven that ATP synthase is

of ERK1/2 (P-X-S/T-P) matched the sequence near the serine 374 site of c-Fos. C and D, the levels of ERK1/2 and phospho-ERK1/2-T202/Y204 were measured using Western blotting. Relative expression levels of phosphorylated ERK1/2 in cells stimulated with Control-CM or MSC-CM were normalized according to the level of total ERK1/2 and the loading control (GAPDH). E and F, the quantified results of Western blotting from three biological replicates are displayed as dot plots. G and H, cell proliferation (G) and cell migration (H) were detected in the lung cancer cells treated with or without MSC-CM in the presence or absence of ERK1/2 inhibitor (SCH772984). All quantified results are shown as mean \pm standard deviation. * $p < 0.05$, ** $p < 0.01$, *** $p < 0.001$, two-tailed t test. CM, conditioned medium; ERK1/2, extracellular signal-regulated protein kinases 1 and 2; MSC, mesenchymal stem cell.

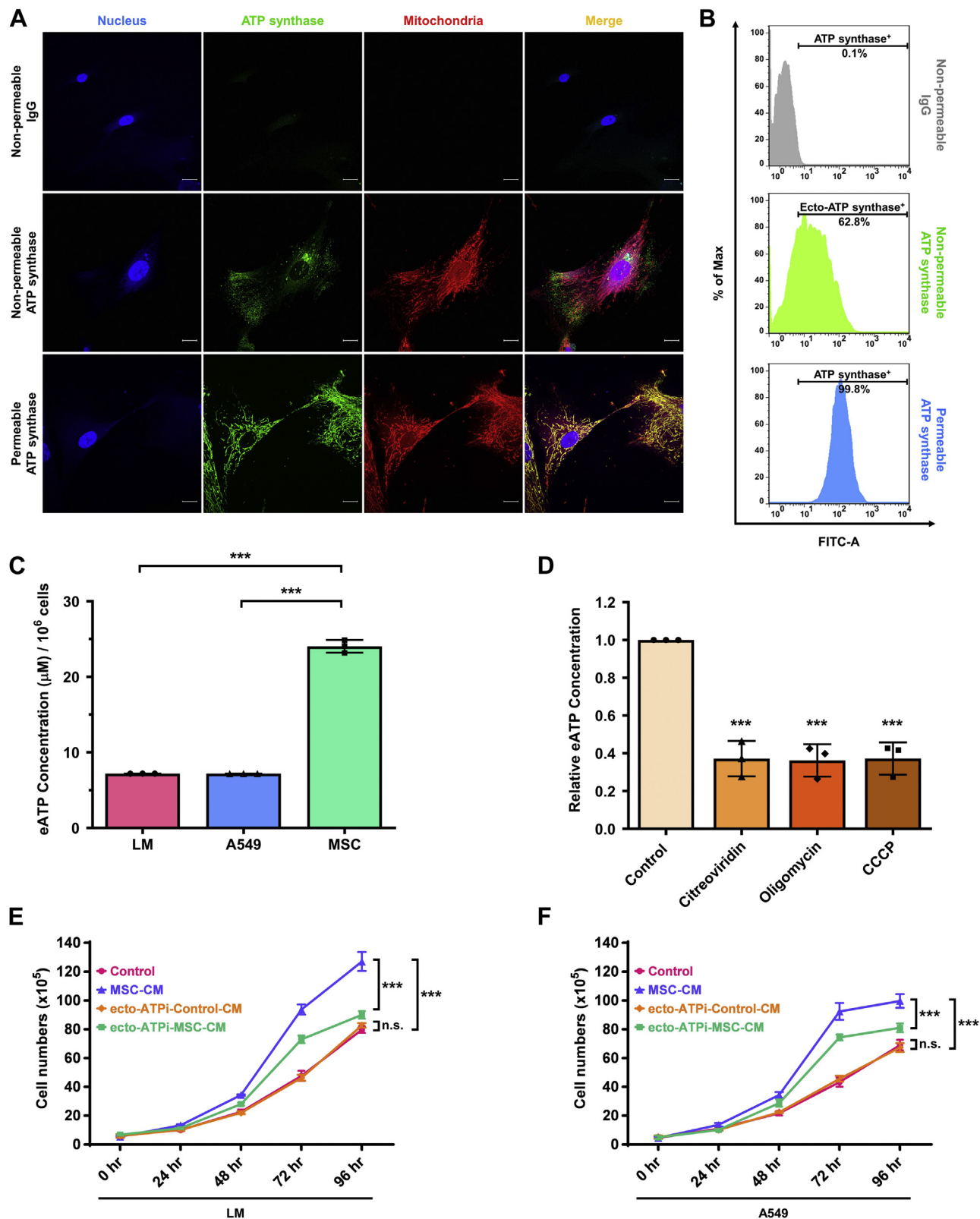


FIG. 5. MSCs secrete extracellular ATP for activation of the ERK1/2-phospho-c-Fos pathway. A, the abundance of cell-surface and mitochondrial ATP synthase was assessed using immunocytochemistry with ATP-synthase-complex antibodies in nonpermeable and permeable MSCs, respectively. MitoTracker Red was used to label the mitochondria, and DAPI was used to stain the nuclei. Scale bar, 20 μm. B, ectopic ATP synthase-positive MSCs were assessed using flow cytometry with antibodies against the ATP synthase complex or control mouse

ectopically expressed on the surface of various cell types (67, 68). This cell-surface ATP synthase, also known as ecto-ATP synthase, contributes to the extracellular production of ATP in normal cells as well as cancer cells (69, 70). To verify whether the accumulating eATP results from ecto-ATP synthase on the cell surface of MSCs, we performed an immunocytochemistry experiment using an antibody against ATP synthase in MSCs. With the cells in their nonpermeabilized form, only any ATP synthase on the cell surface would be detected, and intracellular ATP synthase would not. Cells that were permeabilized using TritonX-100 were used to establish a positive control for the antibody. In contrast, cells incubated with the nonspecific antibody, IgG, did not show any green fluorescent signal. The results showed that the MSCs indeed expressed abundant ecto-ATP synthase, with a punctuated distribution, which was quite different from the distribution observed in mitochondrial networks (Fig. 5A). In contrast, the signal associated with intracellular ATP synthase in the permeabilized MSCs was almost entirely colocalized with the mitochondria. We then wished to know whether ecto-ATP synthase was commonly present on most MSCs. We therefore used flow cytometry to quantify the percentage of ecto-ATP synthase-positive MSCs. The data indicated that approximately 63% of MSCs expressed ecto-ATP synthase (Fig. 5B). An ATP bioluminescence assay also showed that the concentration of eATP in the MSC-CM was consistently higher than that in the CM of the cancer cells (LM-CM and A549-CM; Fig. 5C). This evidence implies that the higher eATP concentration in the TME might result from ecto-ATP synthase on the cell surface of MSCs. To further understand the influence of ecto-ATP synthase at the eATP level, we carried out citreoviridin, oligomycin, and carbonyl cyanide 3-chlorophenylhydrazone as the specific ecto-ATP synthase inhibitors for suppression of eATP release. In previous studies, these ecto-ATP synthase inhibitors are able to significantly decrease the concentration of eATP *via* the specific inhibitory effect on ecto-ATP synthase (20, 29). As shown in Figure 5D, each ecto-ATP synthase inhibitor effectively reduced the concentration of eATP in MSCs, which was consistent with previous studies. Numerous studies point out that ectopic adenylate kinase (ecto-AK) also presents on the cell surface and contributes to the eATP level by catalyzing ATP + AMP from two ADP (71, 72). In order to determine the effect of ecto-AK on eATP production, MSCs pretreated with ecto-ATP synthase inhibitors or a known ecto-AK inhibitor, Ap₅A, were incubated with ADP alone. The eATP formation was only

repressed by Ap₅A after adding ADP (supplemental Fig. S2A). Although these data suggest the eATP level might partially be attributed to the activity of ecto-AK, another piece of evidence determined that the concentration of eATP level was significantly elevated in the presence of both ADP and Pi compared to ADP alone (supplemental Fig. S2B). These data illustrate that ecto-ATP synthase indeed has enzyme activity to promote eATP synthesis. Moreover, treating lung cancer cells with ecto-ATPi-MSC-CM, which contained less eATP, led to a slower proliferation rate than MSC-CM treatment (Fig. 5, E and F). Combining these results, we believe that ecto-ATP synthase on the cell surface of MSCs produces eATP into the TME and leads to the activation of the ERK1/2-c-Fos axis in lung cancer cells.

eATP Secreted by MSCs Regulates Tumor Development via P2X7 Purinergic Receptor Activation

Growing evidence demonstrates that eATP in the TME activates P2 purinergic receptors that are commonly expressed on cancer cells. In the P2X receptor family, P2X purinergic receptor subtype 7 (P2X7R) acts as a central player in cancer development (34, 73, 74). The aforementioned result determined that ATP stimulation activated the phosphorylation of the ERK1/2-c-Fos axis in lung cancer cells (supplemental Fig. S1). We first attempted to uncover whether ATP-induced phosphorylation signaling further regulated proliferation and migration. As shown in supplemental Fig. S3, A and B, ATP treatment increased proliferation rates and motility abilities in LM and A549 lung cancer cells, whereas ATP and a P2X7R antagonist, A 438079, cotreatment reversed these effects. To further understand whether MSCs promote tumor progression by releasing eATP to stimulate P2X7Rs located on the plasma membrane of cancer cells, we used A 438079 to compete with eATP secreted by MSCs. Prior to stimulation with MSC-CM, lung cancer cells were pretreated with A 438079 in order to perform a P2X7R blockade. Western blotting showed that MSC-induced phosphorylation of the ERK1/2-c-Fos axis was abolished by the P2X7R blockade in both LM cells (Fig. 6, A–C) and A549 cells (Fig. 6, D–F). Moreover, the P2X7R blockade also suppressed the cell proliferation (Fig. 6, G and H) and cell migration (Fig. 6, I and J) that was enhanced by MSC-CM treatment. Taken together, these results suggest that eATP secreted by MSCs regulate tumor proliferation and motility *via* activation of the P2X7R-ERK1/2-c-Fos pathway.

IgG. In (A) and (B), MSCs incubated with mouse IgG antibodies served as the negative control, whereas MSCs permeabilized with 0.1% Triton X-100 as the positive control. C, the concentration of extracellular ATP in medium conditioned by lung cancer cells (LM and A549) and MSCs was measured and normalized according to the number of cells present. D, the extracellular ATP in the conditioned medium of MSCs treated with or without the ectopic ATP synthase inhibitors (citreoviridin, oligomycin, and CCCP, respectively) in the presence of ADP and Pi was detected. The relative eATP concentration was normalized according to the number of cells and the control group. E and F, cell proliferation was detected in the LM (E) and A549 (F) lung cancer cells treated with or without MSC-CM in the presence or absence of ecto-ATPi. All quantified results are shown as mean ± standard deviation. **p* < 0.05, ***p* < 0.01, ****p* < 0.001, two-tailed *t* test. CCCP, carbonyl cyanide 3-chlorophenylhydrazone; CM, conditioned medium; LM, low-motility; MSC, mesenchymal stem cell.

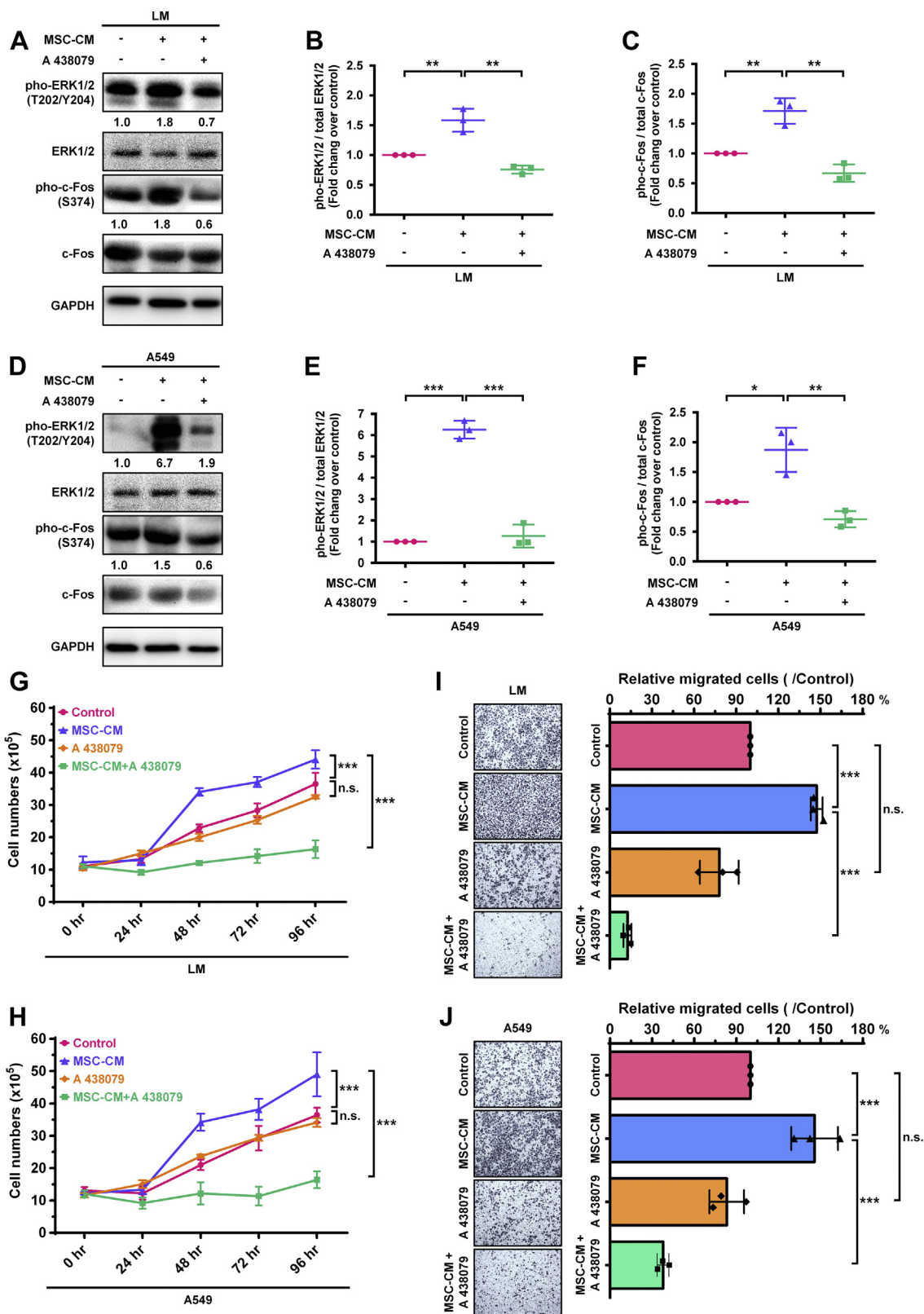


FIG. 6. Inhibition of the P2X7R on lung cancer cells abrogates MSC-CM-triggered tumor proliferation and migration. A–F, the levels of proteins and phosphoproteins of MSC-CM-treated lung cancer cells in the presence or absence of P2X7R inhibitor (A 438079). Relative expression levels of phosphoproteins were normalized according to the levels of total proteins and the loading control (GAPDH) and are shown

DISCUSSION

During the last 10 years, the focus of cancer research has shifted away from the malignant tumor itself and to the TME and its interactions with the tumor. The TME is also thought to play a key role in tumor progression by recruiting stromal cells to provide growth factors and cytokines for tumor cell growth (75). MSCs are one of the stromal cell types in the TME, and emerging data indicate that it can boost tumor development and provide chemoresistance to anticancer drugs (76, 77). In our study, we have demonstrated that MSC-CM improves the cell proliferation and migration abilities of lung cancer cells (Fig. 1). In addition, in order to elucidate the signaling pathways in lung cancer cells that are induced by MSCs, a quantitative phosphoproteomic profiling was performed to reveal MSC-triggered signaling pathway on the MSC-CM treated lung cancer cells (Fig. 2, A–E). The result showed that most of the more significantly expressed kinases are involved in the MAPK pathway, which mediates cell proliferation and cell motility (78, 79). The MAPK cascade plays a key role in the transduction of extracellular signals into cellular responses (78). The MAPKs are classified into three families: extracellular signal-regulated kinase (ERK), Jun amino-terminal kinase (JNK), and p38/stress-activated protein kinase (p38/SAPK). The ERK pathway, also known as the p44/p42 MAPK pathway, is typically upregulated in human tumors and thus represents an attractive target for anticancer drug development (79). Our Western blotting analysis demonstrated that the expression of phospho-ERK1/2-T202/Y204 increased significantly in lung cancer cells stimulated with MSC-CM (Fig. 4, C–F). Moreover, the ERK1/2 inhibitor (SCH772984) abolished MSC-induced cell proliferation and migration in lung cancer cells (Fig. 4, G and H).

The activated ERKs translocate to the nucleus and phosphorylate transcription factors such as c-Fos, c-Jun, c-Myc, Elk-1, Sap-1a, Ets1, Tal, and CREB to regulate tumor progression (78, 80). The c-Fos, a proto-oncogene (81), acts as a member of the activated protein-1 (AP-1) family. It can be dimerized with c-Jun to form the transcription factor activator protein 1 (AP-1) complex, which can bind to DNA at AP-1-specific sites to enhance tumor growth (82, 83). Recent evidence suggests that c-Fos is able to induce the epithelial-mesenchymal transition, leading to epithelial cell invasion and metastasis (84). An increasing number of studies have shown that ERK1/2 enhance the stability of c-Fos by phosphorylating c-Fos at serine 374 (85–90). Herein, we first found that the phosphorylation level of c-Fos doubled in our quantitative phosphoproteomics investigations (Fig. 2E) and the

consensus motif of the ERK1/2 substrate is similar to the sequence near c-Fos Ser374 (Fig. 4, A and B). Our Western blotting results further confirmed that MSCs triggered the MAPK pathway to phosphorylate c-Fos on serine 374 at various time points. We suggest that serine 374 on c-Fos plays a crucial role in MSC-mediated lung cancer cell function (Fig. 3, E–H).

A growing number of studies have reported that ecto-ATP synthase is overexpressed on the cell membrane of various cell types (29, 91). In this study, we surprisingly observed that the whole ATP synthase complex that contains a full complement of subunits was expressed on the cell surface of MSCs using anti-ATP synthase complex immunocapture antibody. This ecto-ATP synthase with functional activity can generate eATP into the lung cancer microenvironment (Fig. 5). P2X7R, one of the receptors in purinergic signaling pathways, presents on the cell membranes of cancer cells, and its expression level is associated with tumor survival, proliferation, and metastasis (33, 35, 44). Several findings show that eATP in the TME can activate the ERK/MAPK pathway via P2X7R stimulation (37, 38, 92). Consistent with these findings, our results indicate that ATP at a concentration of 0.5 mM increased the phosphorylation of c-Fos at serine 374 via activation of the MAPK pathway in lung cancer cells. Moreover, P2X7R blockade reduced MSC-induced c-Fos-S374 phosphorylation in the MAPK pathway of lung cancer cells and functionally downregulated MSC-induced proliferation and migration in lung cancer cells (Fig. 6). Therefore, an in-depth study of the purinergic signaling pathways of the TME may provide us with new cancer therapeutic targets.

Collectively, in this study, we aimed to dissect the role of MSCs in the microenvironment of lung cancer tumors. We discovered that ATP synthase was detected not only on the mitochondria but also on the cell surface of MSCs. As a consequence, ecto-ATP synthase was located on the cell membranes of MSCs and produced eATP into the lung cancer microenvironment. This eATP stimulates the P2X7R on lung cancer cells via ionotropic purinergic signaling. Finally, the eATP in MSC-CM triggered the MAPK pathway to phosphorylate c-Fos at its serine 374 residues to improve c-Fos stability in lung cancer cells. In conclusion, an MSC-derived TME promotes lung cancer cell progression via phosphorylation of c-Fos-S374 in the ERK/MAPK signaling axis (Fig. 7).

DATA AVAILABILITY

Phospho-proteomic profile with MSC-CM stimulation in LM cells data have been deposited to ProteomeXchange (<http://>

as dot plots. G and H, the number of LM cells (G) and A549 cells (H) after treatment with or without MSC-CM in the presence or absence of A 438079 was counted at the indicated time points. I and J, cell migration was assessed in LM cells (I) and A549 cells (J) after treatment with or without MSC-CM in the presence or absence of A 438079. Representative images from three independent experiments are displayed, and the number of migrating cells is shown as mean \pm standard deviation in histogram plots. * $p < 0.05$, ** $p < 0.01$, *** $p < 0.001$, two-tailed t test. CM, conditioned medium; LM, low-motility; MSC, mesenchymal stem cell.

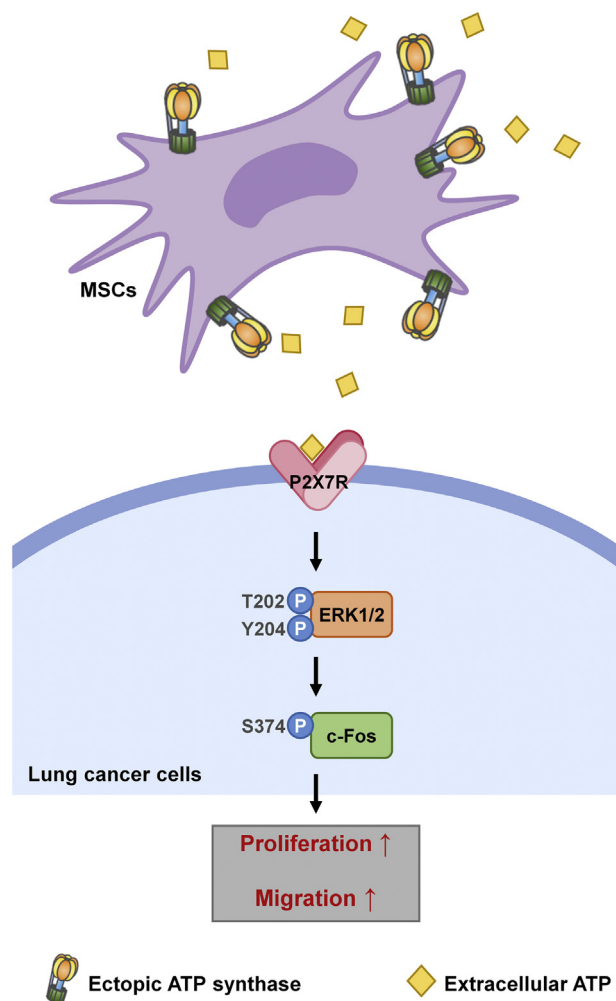


FIG. 7. Schematic diagram of the phosphorylation mechanism induced by MSCs in lung cancer. Ectopic ATP synthase expressed on the cell surface of MSCs secretes extracellular ATP into the tumor microenvironment. This extracellular ATP activates P2X7R on lung cancer cells and subsequently induces the phospho-ERK1/2–phospho-c-Fos axis. The MSCs then contribute to lung cancer development via the promotion of tumor proliferation and migration. ERK1/2, extracellular signal-regulated protein kinases 1 and 2; MSC, mesenchymal stem cell.

www.proteomexchange.org/) via the PRIDE partner repository with the dataset identifier PXD029288.

Supplemental data—This article contains [supplemental data](#).

Acknowledgments—We thank Technology Commons in College of Life Science, National Taiwan University, for technical assistance. We thank Prof. Jia-Lin Lee (Institute of Molecular and Cellular Biology, National Tsing Hua University) for providing LM cells used in this study and Prof. Chia-Lang Hsu (Department of Medical Research, National Taiwan University Hospital) for the constructive suggestions. The schematic figures were created with [BioRender.com](#). We would also like

to thank Uni-edit (www.uni-edit.net) and Anthony Abram for editing and proofreading this manuscript.

Author contributions—Y.-W. C., C.-C. W., C.-F. Y., and C.-H. W. investigation; Y.-W. C. formal analysis; Y.-W. C. and C.-F. Y. visualization; Y.-W. C., C.-C. W., and H.-F. J. writing-original draft; Y.-W. C., H.-C. H., and H.-F. J. writing-review and editing; H.-C. H. and H.-F. J. conceptualization; H.-C. H. and H.-F. J. funding acquisition; H.-C. H. and H.-F. J. project administration.

Funding and additional information—This work was supported by the Ministry of Science and Technology (MOST 107-2314-B-002-254-MY3, MOST 109-2221-E-002-161-MY3, MOST 109-2320-B-002-017-MY3, MOST 109-2221-E-010-012-MY3, and MOST 109-2221-E-010-011-MY3), the Higher Education Sprout Project (NTU-109L8837A).

Conflict of interest—The authors declare that they have no conflict of interest.

Abbreviations—The abbreviations used are: Ap_5A , P^1P^5 -di(adenosine-5') pentaphosphate pentasodium salt; eATP, extracellular ATP; ecto-ATP synthase, ectopic ATP synthase; ERK1/2, extracellular signal-regulated protein kinases 1 and 2; FBS, fetal bovine serum; LM cells, low-motility cells; MAPK, mitogen-activated protein kinase; MSCs, mesenchymal stem cells; MSC-CM, mesenchymal stem cells-conditioned medium; P2X7R, P2X purinergic receptor 7; TME, tumor microenvironment.

Received May 26, 2021, and in revised form, April 1, 2022. Published, MCPRO Papers in Press, April 18, 2022, <https://doi.org/10.1016/j.mcpro.2022.100237>

REFERENCES

- Hanahan, D., and Coussens, L. M. (2012) Accessories to the crime: Functions of cells recruited to the tumor microenvironment. *Cancer Cell* **21**, 309–322
- Whiteside, T. L. (2008) The tumor microenvironment and its role in promoting tumor growth. *Oncogene* **27**, 5904–5912
- Bussard, K. M., Mutkus, L., Stumpf, K., Gomez-Manzano, C., and Marini, F. C. (2016) Tumor-associated stromal cells as key contributors to the tumor microenvironment. *Breast Cancer Res.* **18**, 84
- Yuan, Y., Jiang, Y.-C., Sun, C.-K., and Chen, Q. M. (2016) Role of the tumor microenvironment in tumor progression and the clinical applications. *Oncol. Rep.* **35**, 2499–2515
- Spaeth, E. L., Dembinski, J. L., Sasser, A. K., Watson, K., Klopp, A., Hall, B., Andreeff, M., and Marini, F. (2009) Mesenchymal stem cell transition to tumor-associated fibroblasts contributes to fibrovascular network expansion and tumor progression. *PLoS One* **4**, e4992
- Wang, M., Zhao, J., Zhang, L., Wei, F., Lian, Y., Wu, Y., Gong, Z., Zhang, S., Zhou, J., and Cao, K. (2017) Role of tumor microenvironment in tumorigenesis. *J. Cancer* **8**, 761
- De Palma, M., Biziato, D., and Petrova, T. V. (2017) Microenvironmental regulation of tumour angiogenesis. *Nat. Rev. Cancer* **17**, 457–474
- Hamidi, H., and Ivaska, J. (2018) Every step of the way: Integrins in cancer progression and metastasis. *Nat. Rev. Cancer* **18**, 533–548
- Pittenger, M. F., Mackay, A. M., Beck, S. C., Jaiswal, R. K., Douglas, R., Mosca, J. D., Moorman, M. A., Simonetti, D. W., Craig, S., and Marshak, D. R. (1999) Multilineage potential of adult human mesenchymal stem cells. *Science* **284**, 143

10. Le Blanc, K., and Mougiakakos, D. (2012) Multipotent mesenchymal stromal cells and the innate immune system. *Nat. Rev. Immunol.* **12**, 383–396
11. Ahn, S. Y. (2020) The role of MSCs in the tumor microenvironment and tumor progression. *Anticancer Res.* **40**, 3039
12. Karnoub, A. E., Dash, A. B., Vo, A. P., Sullivan, A., Brooks, M. W., Bell, G. W., Richardson, A. L., Polyak, K., Tubo, R., and Weinberg, R. A. (2007) Mesenchymal stem cells within tumour stroma promote breast cancer metastasis. *Nature* **449**, 557–563
13. Nabha, S. M., dos Santos, E. B., Yamamoto, H. A., Belizi, A., Dong, Z., Meng, H., Saliganan, A., Sabbota, A., Bonfil, R. D., and Cher, M. L. (2008) Bone marrow stromal cells enhance prostate cancer cell invasion through type I collagen in an MMP-12 dependent manner. *Int. J. Cancer* **122**, 2482–2490
14. Duda, D. G., Duyverman, A. M. M. J., Kohno, M., Snuderl, M., Steller, E. J. A., Fukumura, D., and Jain, R. K. (2010) Malignant cells facilitate lung metastasis by bringing their own soil. *Proc. Natl. Acad. Sci. U. S. A.* **107**, 21677
15. Kucerova, L., Matuskova, M., Hlubinova, K., Altanerova, V., and Altaner, C. (2010) Tumor cell behaviour modulation by mesenchymal stromal cells. *Mol. Cancer* **9**, 129
16. Hossain, A., Gumin, J., Gao, F., Figueroa, J., Shinjima, N., Takezaki, T., Priebe, W., Villarreal, D., Kang, S.-G., Joyce, C., Sulman, E., Wang, Q., Marini, F. C., Andreeff, M., Colman, H., et al. (2015) Mesenchymal stem cells isolated from human gliomas increase proliferation and maintain stemness of glioma stem cells through the IL-6/gp130/STAT3 pathway. *Stem Cells* **33**, 2400–2415
17. Wang, M.-L., Pan, C.-M., Chiou, S.-H., Chen, W.-H., Chang, H.-Y., Lee, O. K.-S., Hsu, H.-S., and Wu, C.-W. (2012) Oncostatin M modulates the mesenchymal–epithelial transition of lung adenocarcinoma cells by a mesenchymal stem cell-mediated paracrine effect. *Cancer Res.* **72**, 6051
18. Lin, W.-H., Chang, Y.-W., Hong, M.-X., Hsu, T.-C., Lee, K.-C., Lin, C., and Lee, J.-L. (2021) STAT3 phosphorylation at Ser727 and Tyr705 differentially regulates the EMT–MET switch and cancer metastasis. *Oncogene* **40**, 791–805
19. Chi, S. L., and Pizzo, S. V. (2006) Cell surface F1Fo ATP synthase: A new paradigm? *Ann. Med.* **38**, 429–438
20. Taurino, F., and Gnani, A. (2018) Systematic review of plasma-membrane ecto-ATP synthase: A new player in health and disease. *Exp. Mol. Pathol.* **104**, 59–70
21. Jonckheere, A. I., Smeitink, J. A., and Rodenburg, R. J. (2012) Mitochondrial ATP synthase: Architecture, function and pathology. *J. Inherit. Metab. Dis.* **35**, 211–225
22. Guo, H., Bueler, S. A., and Rubinstein, J. L. (2017) Atomic model for the dimeric FO region of mitochondrial ATP synthase. *Science* **358**, 936–940
23. Moser, T. L., Kenan, D. J., Ashley, T. A., Roy, J. A., Goodman, M. D., Misra, U. K., Cheek, D. J., and Pizzo, S. V. (2001) Endothelial cell surface F₁F₀ ATP synthase is active in ATP synthesis and is inhibited by angiostatin. *Proc. Natl. Acad. Sci. U. S. A.* **98**, 6656
24. Kim, B.-W., Choo, H.-J., Lee, J.-W., Kim, J.-H., and Ko, Y.-G. (2004) Extracellular ATP is generated by ATP synthase complex in adipocyte lipid rafts. *Exp. Mol. Med.* **36**, 476–485
25. Qian, Y., Wang, X., Li, Y., Cao, Y., and Chen, X. (2016) Extracellular ATP a new player in cancer metabolism: NSCLC cells internalize ATP *in vitro* and *in vivo* using multiple endocytic mechanisms. *Mol. Cancer Res.* **14**, 1087
26. Yang, H., Geng, Y.-H., Wang, P., Zhou, Y.-T., Yang, H., Huo, Y.-F., Zhang, H.-Q., Li, Y., He, H.-Y., Tian, X.-X., and Fang, W.-G. (2019) Extracellular ATP promotes breast cancer invasion and epithelial-mesenchymal transition *via* hypoxia-inducible factor 2 α signaling. *Cancer Sci.* **110**, 2456–2470
27. Chi, S. L., Wahl, M. L., Mowery, Y. M., Shan, S., Mukhopadhyay, S., Hilderbrand, S. C., Kenan, D. J., Lipes, B. D., Johnson, C. E., Marusich, M. F., Capaldi, R. A., Dewhirst, M. W., and Pizzo, S. V. (2007) Angiostatin-like activity of a monoclonal antibody to the catalytic subunit of F1F0 ATP synthase. *Cancer Res.* **67**, 4716–4724
28. Zhang, X., Gao, F., Yu, L. L., Peng, Y., Liu, H. H., Liu, J. Y., Yin, M., and Ni, J. (2008) Dual functions of a monoclonal antibody against cell surface F1F0 ATP synthase on both HUVEC and tumor cells. *Acta Pharmacol. Sin.* **29**, 942–950
29. Chang, H. Y., Huang, H. C., Huang, T. C., Yang, P. C., Wang, Y. C., and Juan, H. F. (2012) Ectopic ATP synthase blockade suppresses lung adenocarcinoma growth by activating the unfolded protein response. *Cancer Res.* **72**, 4696–4706
30. Rapaport, E., Fishman, R. F., and Gercel, C. (1983) Growth inhibition of human tumor cells in soft-agar cultures by treatment with low levels of adenosine 5'-triphosphate. *Cancer Res.* **43**, 4402–4406
31. Di Virgilio, F., Sarti, A. C., Falzoni, S., De Marchi, E., and Adinolfi, E. (2018) Extracellular ATP and P2 purinergic signalling in the tumour microenvironment. *Nat. Rev. Cancer* **18**, 601–618
32. Di Virgilio, F. (2012) Purines, purinergic receptors, and cancer. *Cancer Res.* **72**, 5441–5447
33. North, R. A. (2002) Molecular physiology of P2X receptors. *Physiol. Rev.* **82**, 1013–1067
34. Di Virgilio, F., and Adinolfi, E. (2016) Extracellular purines, purinergic receptors and tumor growth. *Oncogene* **36**, 293
35. Adinolfi, E., Callegari, M. G., Ferrari, D., Bolognesi, C., Minelli, M., Wieckowski, M. R., Pinton, P., Rizzuto, R., and Di Virgilio, F. (2005) Basal activation of the P2X7 ATP receptor elevates mitochondrial calcium and potential, increases cellular ATP levels, and promotes serum-independent growth. *Mol. Biol. Cell* **16**, 3260–3272
36. Vázquez-Cuevas, F. G., Martínez-Ramírez, A. S., Robles-Martínez, L., Garay, E., García-Carrancá, A., Pérez-Montiel, D., Castañeda-García, C., and Arellano, R. O. (2014) Paracrine stimulation of P2X7 receptor by ATP activates a proliferative pathway in ovarian carcinoma cells. *J. Cell. Biochem.* **115**, 1955–1966
37. Chen, S., Ma, Q., Krafft, P. R., Chen, Y., Tang, J., Zhang, J., and Zhang, J. H. (2013) P2X7 receptor antagonism inhibits p38 mitogen-activated protein kinase activation and ameliorates neuronal apoptosis after subarachnoid hemorrhage in rats. *Crit. Care Med.* **41**, e466–e474
38. Young, C. N. J., and Górecki, D. C. (2018) P2RX7 purinoceptor as a therapeutic target—the second coming? *Front. Chem.* **6**, 248
39. Nuka, E., Ohnishi, K., Terao, J., and Kawai, Y. (2018) ATP/P2X7 receptor signaling as a potential anti-inflammatory target of natural polyphenols. *PLoS One* **13**, e0204229
40. Gu, B. J., and Wiley, J. S. (2006) Rapid ATP-induced release of matrix metalloproteinase 9 is mediated by the P2X₇ receptor. *Blood* **107**, 4946–4953
41. Jelassi, B., Chantôme, A., Alcaraz-Pérez, F., Baroja-Mazo, A., Cayuela, M. L., Pelegrin, P., Surprenant, A., and Roger, S. (2011) P2X7 receptor activation enhances SK3 channels- and cystein cathepsin-dependent cancer cells invasiveness. *Oncogene* **30**, 2108
42. Di Virgilio, F., Falzoni, S., Giuliani, A. L., and Adinolfi, E. (2016) P2 receptors in cancer progression and metastatic spreading. *Curr. Opin. Pharmacol.* **29**, 17–25
43. Roger, S., and Pelegrin, P. (2011) P2X7 receptor antagonism in the treatment of cancers. *Expert. Opin. Investig. Drugs* **20**, 875–880
44. Adinolfi, E., Raffaghello, L., Giuliani, A. L., Cavazzini, L., Capece, M., Chiozzi, P., Bianchi, G., Kroemer, G., Pistoia, V., and Di Virgilio, F. (2012) Expression of P2X7 receptor increases *in vivo* tumor growth. *Cancer Res.* **72**, 2957–2969
45. Hung, C. J., Yao, C. L., Cheng, F. C., Wu, M. L., Wang, T. H., and Hwang, S. M. (2010) Establishment of immortalized mesenchymal stromal cells with red fluorescence protein expression for *in vivo* transplantation and tracing in the rat model with traumatic brain injury. *Cytotherapy* **12**, 455–465
46. Chang, Y.-W., Su, Y.-J., Hsiao, M., Wei, K.-C., Lin, W.-H., Liang, C.-J., Chen, S.-C., and Lee, J.-L. (2015) Diverse targets of β -catenin during the epithelial–mesenchymal transition define cancer stem cells and predict disease relapse. *Cancer Res.* **75**, 3398
47. Masuda, T., Tomita, M., and Ishihama, Y. (2008) Phase transfer surfactant-aided trypsin digestion for membrane proteome analysis. *J. Proteome Res.* **7**, 731–740
48. Yeung, Y.-G., and Stanley, E. R. (2010) Rapid detergent removal from peptide samples with ethyl acetate for mass spectrometry analysis. *Curr. Protoc. Protein Sci.* **Chapter 16**. Unit-16.12
49. Rappsilber, J., Mann, M., and Ishihama, Y. (2007) Protocol for micro-purification, enrichment, pre-fractionation and storage of peptides for proteomics using StageTips. *Nat. Protoc.* **2**, 1896–1906
50. Boersema, P. J., Raijmakers, R., Lemeer, S., Mohammed, S., and Heck, A. J. (2009) Multiplex peptide stable isotope dimethyl labeling for quantitative proteomics. *Nat. Protoc.* **4**, 484–494
51. Sugiyama, N., Masuda, T., Shinoda, K., Nakamura, A., Tomita, M., and Ishihama, Y. (2007) Phosphopeptide enrichment by aliphatic hydroxy

- acid-modified metal oxide chromatography for nano-LC-MS/MS in proteomics applications. *Mol. Cell. Proteomics* **6**, 1103–1109
52. Kyono, Y., Sugiyama, N., Imami, K., Tomita, M., and Ishihama, Y. (2008) Successive and selective release of phosphorylated peptides captured by hydroxy acid-modified metal oxide chromatography. *J. Proteome Res.* **7**, 4585–4593
 53. Chang, Y. W., Hsu, C. L., Tang, C. W., Chen, X. J., Huang, H. C., and Juan, H. F. (2020) Multiomics reveals ectopic ATP synthase blockade induces cancer cell death via a lncRNA-mediated phospho-signaling network. *Mol. Cell. Proteomics* **19**, 1805–1825
 54. Cox, J., Neuhauser, N., Michalski, A., Scheltema, R. A., Olsen, J. V., and Mann, M. (2011) Andromeda: A peptide search engine integrated into the MaxQuant environment. *J. Proteome Res.* **10**, 1794–1805
 55. Cox, J., and Mann, M. (2008) MaxQuant enables high peptide identification rates, individualized p.p.b.-range mass accuracies and proteome-wide protein quantification. *Nat. Biotechnol.* **26**, 1367–1372
 56. Tyanova, S., Temu, T., Sinitcyn, P., Carlson, A., Hein, M. Y., Geiger, T., Mann, M., and Cox, J. (2016) The Perseus computational platform for comprehensive analysis of (prote)omics data. *Nat. Methods* **13**, 731–740
 57. Lachmann, A., and Ma'ayan, A. (2009) Kea: Kinase enrichment analysis. *Bioinformatics* **25**, 684–686
 58. Aggeler, R., Coons, J., Taylor, S. W., Ghosh, S. S., Garcia, J. J., Capaldi, R. A., and Marusich, M. F. (2002) A functionally active human F1F0 ATPase can be purified by immunocapture from heart tissue and fibroblast cell lines. Subunit structure and activity studies. *J. Biol. Chem.* **277**, 33906–33912
 59. Ridge, S. M., Sullivan, F. J., and Glynn, S. A. (2017) Mesenchymal stem cells: Key players in cancer progression. *Mol. Cancer* **16**, 31
 60. Lee, M. W., Ryu, S., Kim, D. S., Lee, J. W., Sung, K. W., Koo, H. H., and Yoo, K. H. (2019) Mesenchymal stem cells in suppression or progression of hematologic malignancy: Current status and challenges. *Leukemia* **33**, 597–611
 61. Raman, M., Chen, W., and Cobb, M. H. (2007) Differential regulation and properties of MAPKs. *Oncogene* **26**, 3100–3112
 62. Johnson, G. L., and Lapadat, R. (2002) Mitogen-activated protein kinase pathways mediated by ERK, JNK, and p38 protein kinases. *Science* **298**, 1911
 63. Meloche, S., and Pouyssegur, J. (2007) The ERK1/2 mitogen-activated protein kinase pathway as a master regulator of the G1- to S-phase transition. *Oncogene* **26**, 3227–3239
 64. Morris, E. J., Jha, S., Restaino, C. R., Dayananth, P., Zhu, H., Cooper, A., Carr, D., Deng, Y., Jin, W., Black, S., Long, B., Liu, J., Dinunzio, E., Windsor, W., Zhang, R., et al. (2013) Discovery of a novel ERK inhibitor with activity in models of acquired resistance to BRAF and MEK inhibitors. *Cancer Discov.* **3**, 742–750
 65. Stagg, J., and Smyth, M. J. (2010) Extracellular adenosine triphosphate and adenosine in cancer. *Oncogene* **29**, 5346–5358
 66. Yang, H., Geng, Y.-H., Wang, P., Yang, H., Zhou, Y.-T., Zhang, H.-Q., He, H.-Y., Fang, W.-G., and Tian, X.-X. (2020) Extracellular ATP promotes breast cancer invasion and chemoresistance via SOX9 signaling. *Oncogene* **39**, 5795–5810
 67. Moser, T. L., Stack, M. S., Asplin, I., Enghild, J. J., Højrup, P., Everitt, L., Hubchak, S., Schnaper, H. W., and Pizzo, S. V. (1999) Angiostatin binds ATP synthase on the surface of human endothelial cells. *Proc. Natl. Acad. Sci. U. S. A.* **96**, 2811
 68. Martinez, L. O., Jacquet, S., Esteve, J.-P., Rolland, C., Cabezón, E., Champagne, E., Pineau, T., Georgeaud, V., Walker, J. E., Tercé, F., Collet, X., Perret, B., and Barbaras, R. (2003) Ectopic β -chain of ATP synthase is an apolipoprotein A-I receptor in hepatic HDL endocytosis. *Nature* **421**, 75–79
 69. Chi, S. L., and Pizzo, S. V. (2006) Angiostatin is directly cytotoxic to tumor cells at low extracellular pH: A mechanism dependent on cell surface-associated ATP synthase. *Cancer Res.* **66**, 875
 70. Xing, S. L., Yan, J., Yu, Z. H., and Zhu, C. Q. (2011) Neuronal cell surface ATP synthase mediates synthesis of extracellular ATP and regulation of intracellular pH. *Cell Biol. Int.* **35**, 81–86
 71. Quillen, E. E., Haslam, G. C., Samra, H. S., Amani-Taleshi, D., Knight, J. A., Wyatt, D. E., Bishop, S. C., Colvert, K. K., Richter, M. L., and Kitos, P. A. (2006) Ectoadenylate kinase and plasma membrane ATP synthase activities of human vascular endothelial cells. *J. Biol. Chem.* **281**, 20728–20737
 72. Mangiullo, R., Gnoni, A., Leone, A., Gnoni, G. V., Papa, S., and Zanotti, F. (2008) Structural and functional characterization of FoF1-ATP synthase on the extracellular surface of rat hepatocytes. *Biochim. Biophys. Acta* **1777**, 1326–1335
 73. Idzko, M., Ferrari, D., and Eltzschig, H. K. (2014) Nucleotide signalling during inflammation. *Nature* **509**, 310
 74. Di Virgilio, F., Dal Ben, D., Sarti, A. C., Giuliani, A. L., and Falzoni, S. (2017) The P2X7 receptor in infection and inflammation. *Immunity* **47**, 15–31
 75. Cirri, P., and Chiarugi, P. (2011) Cancer associated fibroblasts: The dark side of the coin. *Am. J. Cancer Res.* **1**, 482–497
 76. Seke Etet, P. F., Vecchio, L., and Nwabo Kamdje, A. H. (2012) Signaling pathways in chronic myeloid leukemia and leukemic stem cell maintenance: Key role of stromal microenvironment. *Cell. Signal.* **24**, 1883–1888
 77. Nwabo Kamdje, A. H., Kamga, P. T., Simo, R. T., Vecchio, L., Seke Etet, P. F., Muller, J. M., Bassi, G., Lukong, E., Goel, R. K., Armvene, J. M., and Kramer, M. (2017) Mesenchymal stromal cells' role in tumor microenvironment: Involvement of signaling pathways. *Cancer Biol. Med.* **14**, 129–141
 78. Zhang, W., and Liu, H. T. (2002) MAPK signal pathways in the regulation of cell proliferation in mammalian cells. *Cell Res.* **12**, 9
 79. Kohno, M., and Pouyssegur, J. (2006) Targeting the ERK signaling pathway in cancer therapy. *Ann. Med.* **38**, 200–211
 80. Chang, F., Steelman, L. S., Lee, J. T., Shelton, J. G., Navolanic, P. M., Blalock, W. L., Franklin, R. A., and McCubrey, J. A. (2003) Signal transduction mediated by the Ras/Raf/MEK/ERK pathway from cytokine receptors to transcription factors: Potential targeting for therapeutic intervention. *Leukemia* **17**, 1263–1293
 81. Basset-Séguin, N., Escot, C., Molès, J. P., Blanchard, J. M., Kerai, C., and Guilhou, J. J. (1991) C-fos and c-jun proto-oncogene expression is decreased in psoriasis: An *in situ* quantitative analysis. *J. Invest. Dermatol.* **97**, 672–678
 82. Chiu, R., Boyle, W. J., Meek, J., Smeal, T., Hunter, T., and Karin, M. (1988) The c-fos protein interacts with c-Jun/AP-1 to stimulate transcription of AP-1 responsive genes. *Cell* **54**, 541–552
 83. Angel, P., and Karin, M. (1991) The role of Jun, Fos and the AP-1 complex in cell-proliferation and transformation. *Biochim. Biophys. Acta* **1072**, 129–157
 84. Fialka, I. (1996) The estrogen-dependent c-JunER protein causes a reversible loss of mammary epithelial cell polarity involving a destabilization of adherens junctions. *J. Cell Biol.* **132**, 1115–1132
 85. Wang, Y., and Prywes, R. (2000) Activation of the c-fos enhancer by the erk MAP kinase pathway through two sequence elements: The c-fos AP-1 and p62TCF sites. *Oncogene* **19**, 1379–1385
 86. Monje, P., Hernandez-Losa, J., Lyons, R. J., Castellone, M. D., and Gutkind, J. S. (2005) Regulation of the transcriptional activity of c-Fos by ERK. A novel role for the prolyl isomerase PIN1. *J. Biol. Chem.* **280**, 35081–35084
 87. Gilley, R., March, H. N., and Cook, S. J. (2009) ERK1/2, but not ERK5, is necessary and sufficient for phosphorylation and activation of c-Fos. *Cell. Signal.* **21**, 969–977
 88. Deng, T., and Karin, M. (1994) c-Fos transcriptional activity stimulated by H-Ras-activated protein kinase distinct from JNK and ERK. *Nature* **371**, 171–175
 89. Okazaki, K., and Sagata, N. (1995) The Mos/MAP kinase pathway stabilizes c-Fos by phosphorylation and augments its transforming activity in NIH 3T3 cells. *EMBO J.* **14**, 5048–5059
 90. Gupta, S., Campbell, D., Derijard, B., and Davis, R. J. (1995) Transcription factor ATF2 regulation by the JNK signal transduction pathway. *Science* **267**, 389
 91. Li, W., Li, Y., Li, G., Zhou, Z., Chang, X., Xia, Y., Dong, X., Liu, Z., Ren, B., Liu, W., and Li, Y. (2017) Ectopic expression of the ATP synthase beta subunit on the membrane of PC-3M cells supports its potential role in prostate cancer metastasis. *Int. J. Oncol.* **50**, 1312–1320
 92. Baricordi, O. R., Melchiorri, L., Adinolfi, E., Falzoni, S., Chiozzi, P., Buell, G., and Di Virgilio, F. (1999) Increased proliferation rate of Lymphoid cells transfected with the P2X7 ATP receptor. *J. Biol. Chem.* **274**, 33206–33208